Neutron Supermirrors: Design and Application

Ch. Rehm, M. Agamalian, F. Klose
Oak Ridge National Laboratory, Spallation Neutron Source Project

Neutron supermirrors are used to efficiently transport neutrons from a source to a scattering instrument. This report reviews basic principles and utilization of such supermirrors, and consists of two sections: Firstly, a general introduction to supermirrors is given, introducing recipes for supermirror design, and studying the influence of various design parameters. Secondly, it is discussed how the performance of modern neutron scattering instruments depends on the efficiency of supermirrors.

May 2002

1. Introduction

It is well known that neutron scattering is a powerful tool for the study of condensed matter because the wavelengths and energies of thermal and cold neutrons match well to the length and energy scales of solids and liquids.[1] The applicability of neutron scattering techniques, however, is limited by the relatively low flux of useful neutrons generated by today's research reactors or pulsed spallation sources, which is many orders of magnitude smaller than the flux of X-rays produced by contemporary photon sources. Recently, major efforts have been made to optimize existing sources and to develop new more powerful sources. The Spallation Neutron Source (SNS), which is already under construction at Oak Ridge National Laboratory, will become operational in 2006, and generate an effective neutron flux about one order of magnitude higher than the best existing neutron sources. Other approaches to gain intensity concern optimization of neutron optical components, development of new optical devices, and implementation of advanced instrument designs.[2] Simulation calculations indicate that these approaches should further increase the flux by up to one order of magnitude for particular SNS scattering instruments. The total intensity gain for SNS instruments, therefore, can be as high as two orders of magnitude, which will greatly enhance the quality of neutron scattering studies.

Fig. 1 shows the SNS spectrometers and diffractometers to be built, and how they are grouped around the target providing each instrument with neutrons.

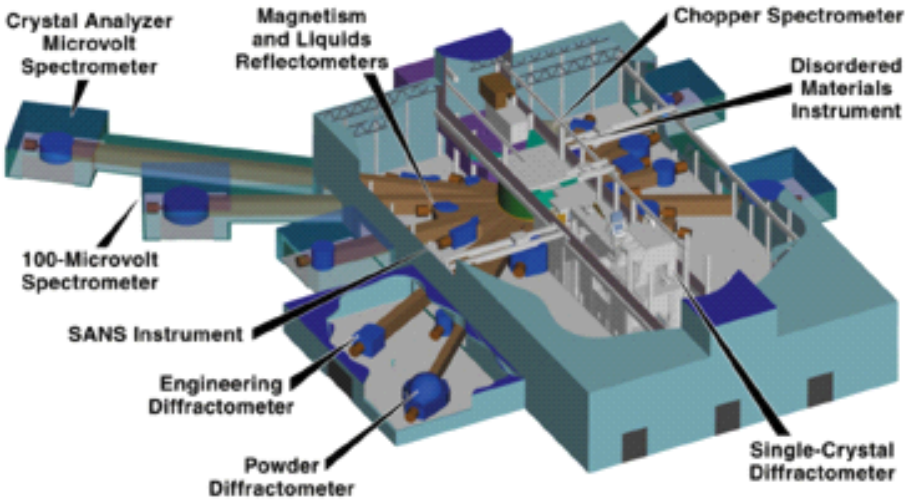

Fig. 1
SNS spectrometers and diffractometers

2. Neutron transportation

After neutrons have been produced in the source and moderated to useful energies, they need to be delivered to a variety of instruments, typically over a distance r, of some tens of meters. Fig. 2 shows a sketch of the experimental set-up for a typical neutron scattering instrument. In the simplest case, an evacuated tube could be employed for transporting the neutron beam. This approach, however, would deliver only those neutrons to the sample with direct line-of-sight paths, resulting in very little neutron flux at the sample position (the neutron flux decreases with $1/r^2$).

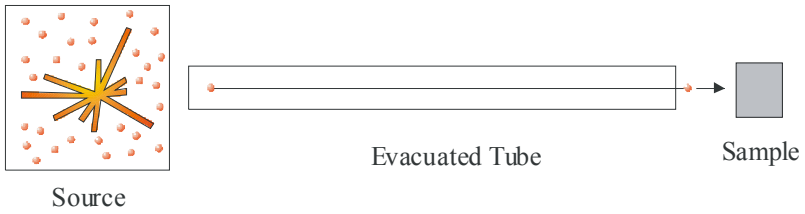

Fig. 2
Neutron transport through an evacuated tube

By using "neutron guides", however, much higher flux on the sample can be achieved.[3]

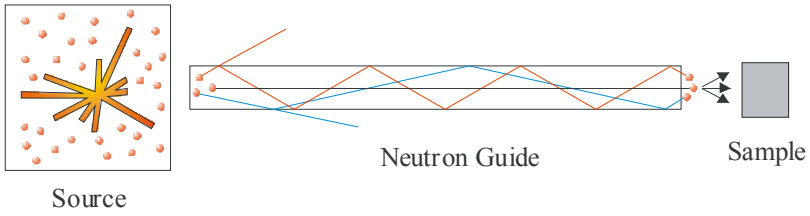

Fig. 3
Neutron transport through a neutron guide

Neutron guides typically consist of rectangular glass tubes internally coated with thin metal films. The guides are up to 100 m long, and typically made of 0.5-1 m long segments, fabricated and adjusted to high precision. The segments are usually constructed from polished glass plates (with a typical thickness of ~1-2 cm).

Fig. 4
Glass channel neutron guide[4]

Borated glass is often chosen as substrate material because of its neutron absorbing capabilities (of course, thermal and cold neutrons only). It prevents neutrons that are not reflected by the coating from escaping the guide channel. Released neutrons may cause activation problems in materials used for vacuum housing, alignment fixtures and shielding in the vicinity of the guide. Another advantage of borated glass is that it prevents neutrons which have thermalized in the shielding around the guide from re-entering. This feature is particularly important for guides at pulsed sources where thermalized neutron background would interfere with time-of-flight measurements.

In high-energy neutron radiation environments, i.e. very close to a moderator, however, glass failures (cracking) have been reported for borated glass.

The requirement for rms-roughness of the substrate is typically 3-5 Å. Some guide designs are using very cost-effective float-glass plates which naturally have such very low roughness. The drawback of float-glass is that the long-range roughness ("waviness") often is insufficient (neutron guide specifications typically ask for < 1.5 mrad maximum deviation of any area on the surface relative to overall glass surface). Therefore, it is necessary that the vendor sorts out all plates before coating which do not fulfill this requirement. Additionally, the deposition process itself can result in strain leading to surface bending. In this case the flatness may be restored by pressing the glass pieces against very flat reference surfaces during the gluing process.

Another drawback of float-glass is that the surfaces and the long-range flatness are particularly good only for a plate thickness close to 3-5 mm (vendor info). If one attempts to pull vacuum directly on float-glass guides, the mechanical stability might be questionable. In these cases, one often uses an external vacuum housing (for example a steel casing).

Neutron guide coatings work based on the principle of total reflection.

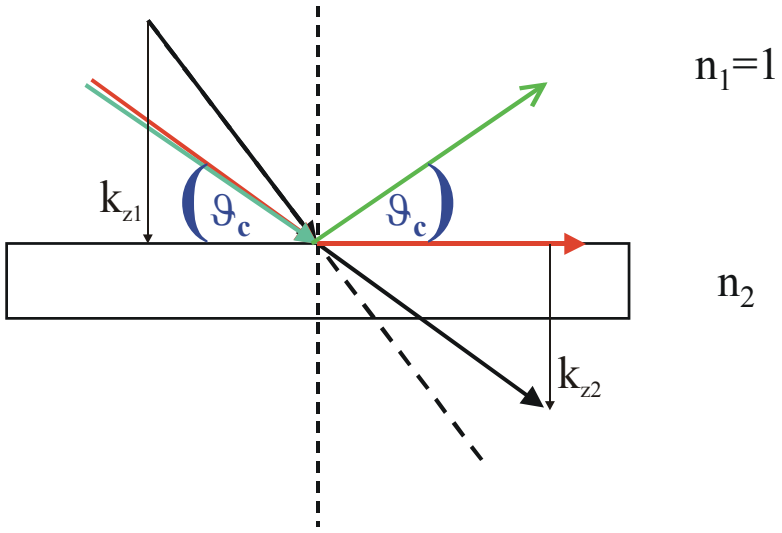

Fig. 5
The principle of total reflection

Fig. 5 shows an example for a reflection process. Very important for optical properties of matter is the refractive index n. It is the ratio of the corresponding perpendicular wave vector components k_{z2} and k_{z1} when a neutron passes an interface between vacuum and matter.

Assume a neutron beam traveling within vacuum ($n_1 = 1$). n_2 is the refractive index of the sample material. In case n_1 is larger than n_2, the neutron beam will be refracted away from the normal direction (black arrow). Inside the material, the perpendicular component of the neutron wave vector is reduced to k_{z2} compared to its value k_{z1} outside the material. If the angle of the incident neutron beam becomes smaller, a so-called evanescent wave traveling along the surface is created (red arrow). A further decrease of the angle of incidence leads to total reflection. The incoming radiation practically cannot penetrate the material (green arrow). The angle of incidence at which total reflection occurs, is called the critical angle ϑ_c.

ϑc is determined by the refractive index, which depends on neutron wavelength and on scattering length density of the reflecting material. For any given material, ϑc can be calculated as

$$\vartheta_c(\lambda) = \sqrt{2[1-n(\lambda)]} = \sqrt{\frac{N \cdot b}{\pi}} \cdot \lambda \qquad (1)$$

where n is the refractive index, λ the neutron wavelength, and $N \cdot b$ the product of number density N [atoms per unit volume], and scattering length b of the material. $N \cdot b$ is usually referred to as scattering length density.

Since TOF instrumentation typically involves a large range of neutron wavelength, it is more appropriate to convert the critical angle into the corresponding critical momentum transfer

$$q_c = \frac{4 \cdot \pi \cdot \sin\theta_c}{\lambda} = 4\sqrt{N \cdot b \cdot \pi} \qquad (2)$$

If the interior of the guide is coated with pure Ni, all neutrons hitting its surfaces at angles lower than the critical angle of Ni (ϑ_c^{Ni}/λ = 1.7 mrad/Å) will be totally reflected. Such a neutron guide coating is usually defined as "m=1" mirror. In order to increase the critical angle of a coating, resulting in higher guide transmission, the reflecting Ni layer should be substituted by so-called "supermirrors". Supermirror coatings consist of multilayers composed of thin films of materials showing large contrast in scattering length density, for example Ni and Ti.[5] The performance of a supermirror (SM) is described by the increase of its q_c-value compared to natural Ni:

$$q_c^{SM} = m \times q_c^{Ni} \qquad (3)$$

When using neutron guides, the gained flux consists of distribution of neutrons which have a higher degree of divergence compared to those having "natural divergence" (neutrons that would reach the sample if no guide were present). In the beginning, natural Ni, the element having the largest angle for total reflection for a given neutron wavelength, was employed as coating. Nowadays, more sophisticated "supermirror" coatings are used, as will be discussed below. The choice for a particular coating and a particular geometry for the guide system strongly depend on the requirements of the specific instrument that is fed by the guide and, of course, by financial constraints. In some cases high performance supermirrors are required, while in others Ni coatings are sufficient.

Neutron guides in pulsed facilities often differ from their reactor-based counterparts due to time-of-flight (TOF) based instrument operation. At reactors, long guide systems are employed for cold neutron research, and generally several instruments are fed by a single guide. In contrast, most SNS instruments that are currently being designed occupy single beam ports. Many instruments, such as reflectometers and small-angle scattering machines, can take advantage of a relatively wide neutron bandwidth for their operation. Because of this, it is advantageous to build these instruments relatively short, typically 15-20 m. Key optical components of these instruments are channel beam deflectors ("beam benders") and focusing guides. Beam benders are used for losing the direct-line-of-sight to the moderator quickly in order to reduce the associated background radiation of high-energy neutrons and gammas; focusing guides spatially compress the beam and therefore enhance the neutron flux per sample area. The compact design of these devices requires supermirrors with very high critical angles for total reflection.

3. Theoretical determination of reflectivity

This chapter explains how reflectivity of a given material can be calculated.

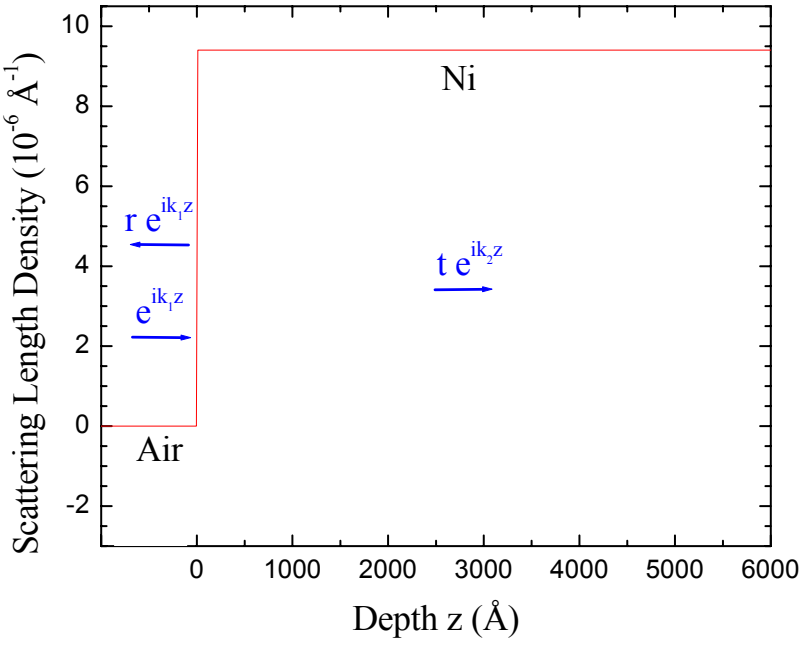

Fig. 6
Scattering length density profile of air/Ni

Fig. 6 shows the scattering length density profile of air/Ni. e^{ikz} characterizes the incident beam, r the amplitude of the reflected beam, and t the amplitude of the transmitted beam, respectively. k_1 and k_2 are the z-projections of the wave vector of the incoming (within air) and transmitted (within Ni) beam, respectively.

Using the Fresnel equations, reflectivity and transmission at the air/Ni interface can be calculated according to

$$\text{Reflectivity} \quad R = |r|^2 = \left| \frac{k_1 - k_2}{k_1 + k_2} \cdot e^{i2k_1 z} \right|^2$$

$$\text{Transmission} \quad T = |t|^2 = \left| \frac{2k_1}{k_1 + k_2} \cdot e^{i2(k_1 - k_2)z} \right|^2$$

In case of a multilayer sample with [500 Å Ni / 500 Å Ti]*4 deposited on a Si substrate, reflectivity and transmission have to be calculated at each individual interface, see Fig. 7.

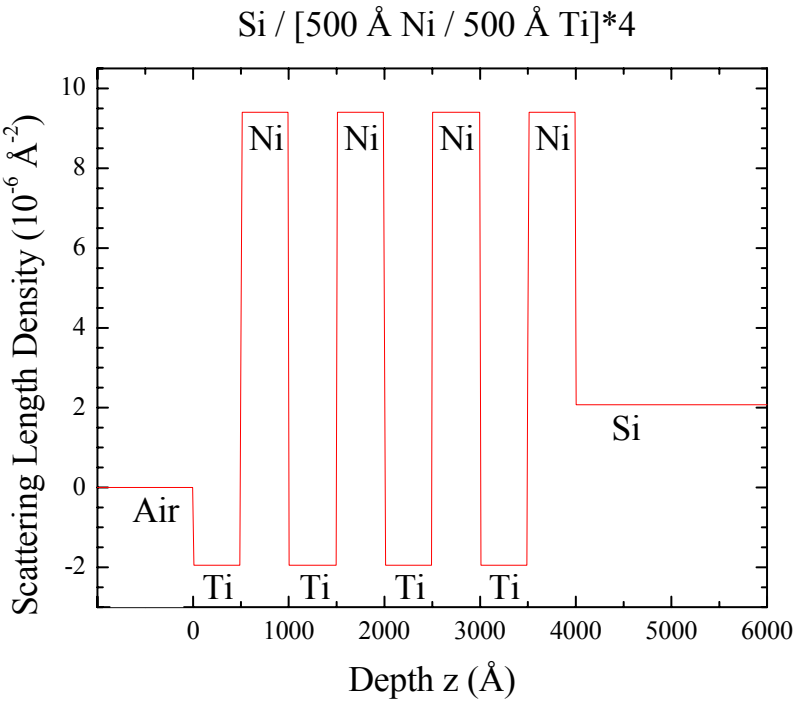

Fig. 7
Scattering length density profile of
*Si / [500 Å Ni / 500 Å Ti]*4*

Roughness can be taken into account by two different ways:

i) Debye-Waller factor
Névot and Croce suggested to include rms-roughnesses σ_i in the Fresnel coefficient as an effective Debye-Waller factor:[6]

$$R_i = R_i^{\text{Fresnel}} \cdot e^{-2q^2 \cdot \sigma_{i+1}^2}$$

Note that a different σ may be applied at each individual interface.

ii) Approach the interface concentration profile by small steps of regions with constant concentration.

Simulation calculations of neutron reflectivity were done by using the program *Parratt*[7] where absorption, incoherent scattering, and interdiffusion/roughness (as described in i) are taken into account, see screenshot shown in Fig. 8.

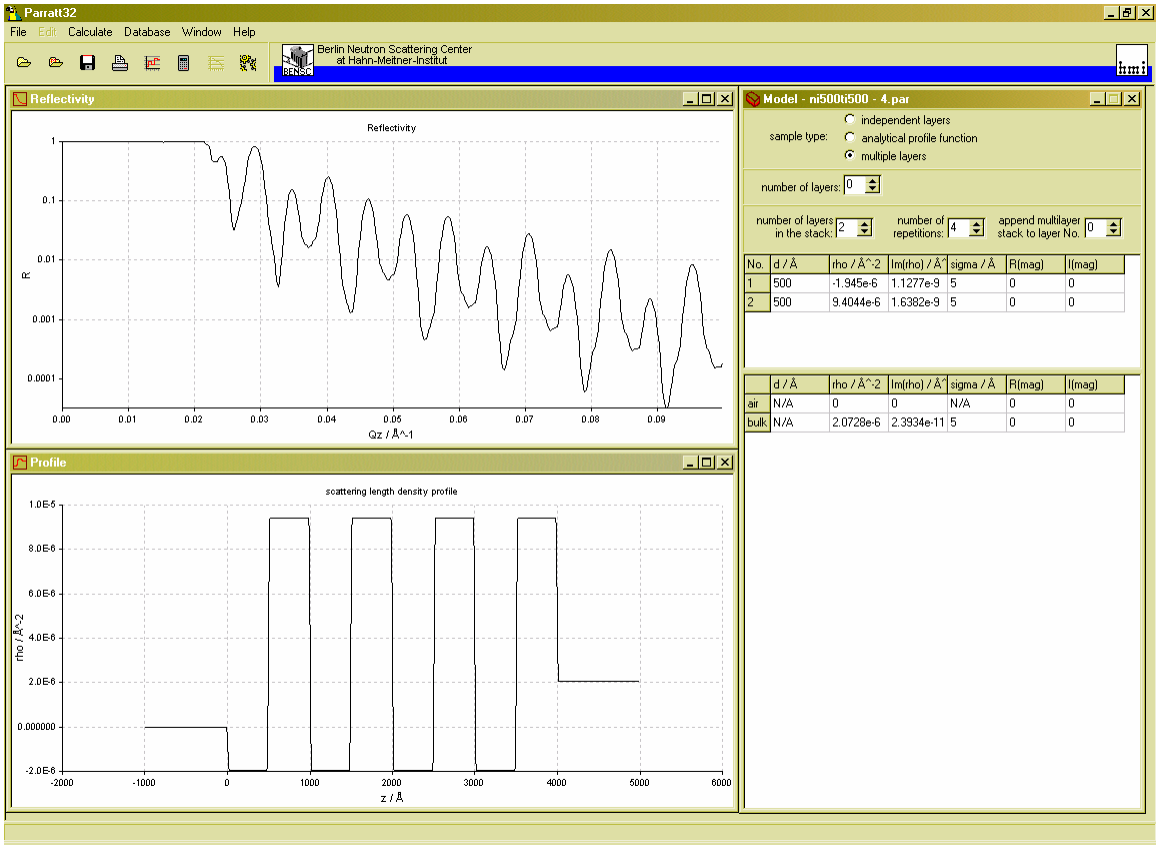

Fig. 8
*Neutron reflectivity and scattering length density profile of a [500 Å Ni / 500 Å Ti]*4 multilayer calculated with Parratt*[6]

Input parameters are:

d:	Thickness of the layer [Å]
rho:	Scattering length density [$Å^{-2}$]; for neutrons: $N \cdot b_{real}$
Im(rho):	Imaginary part (absorption) plus incoherent scattering length density [$Å^{-2}$];
sigma:	Interfacial roughness [Å]

4. Neutron guide coating

4.1 Basic design idea

For neutron guide coatings, materials with a large critical angle ϑ_c for total reflection and high reflectivity are needed.

Since the critical angle is directly proportional to the scattering length density, the most valuable candidate for supermirror material is Ni. Ni shows the highest scattering length density of all natural elements.

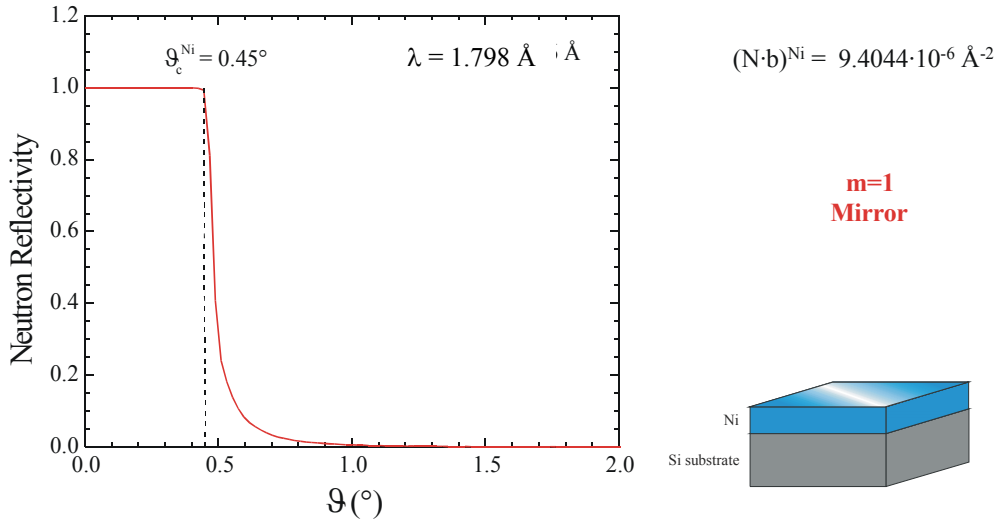

Fig. 9
Neutron reflectivity of Si / 1000 Å Ni for λ = 1.798 Å

Fig. 9 shows the theoretical neutron reflectivity from a 1000 Å thick Ni layer on a Si substrate. Up to the critical angle (for the given wavelength λ = 1.798 Å) of ϑ_c = 0.45°, the neutron reflectivity is very close to unity then it drops.

If the coating is done with pure Ni, all neutrons hitting the surface under an angle lower than ϑ_c will be totally reflected. In that case the mirror is described as an m=1 quality.

There are minor reflectivity losses due to absorption and incoherent scattering, and possible further reductions due to roughness and small-angle scattering, which will not be further discussed here.

In order to increase ϑ_c of a coating (resulting in more neutrons being totally reflected during their way through the neutron guide), one has to switch to another system instead of a pure Ni layer, namely to depth-graded multilayer systems or so-called "supermirrors", see Fig. 10.

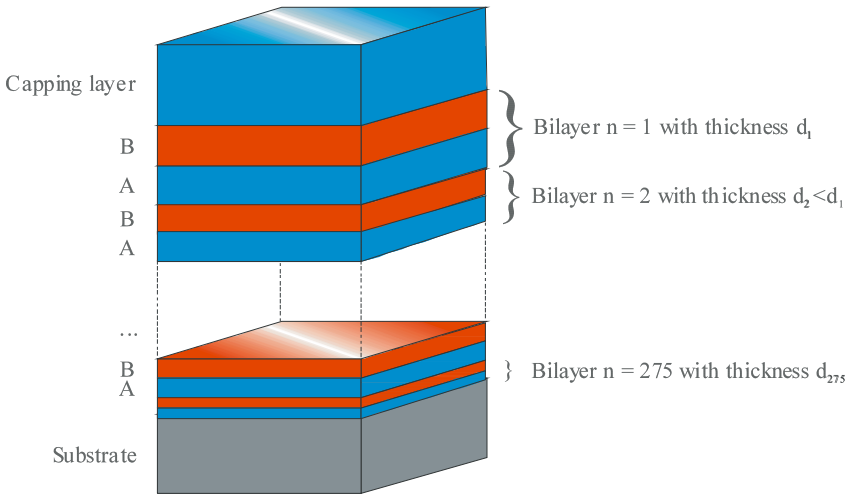

Fig. 10
Schematic composition of a depth-graded A/B multilayer deposited on a substrate

Fig. 11 shows schematically how the angle for total reflection can be increased beyond the critical angle ϑ_c of Ni by using a depth-graded multilayer system.

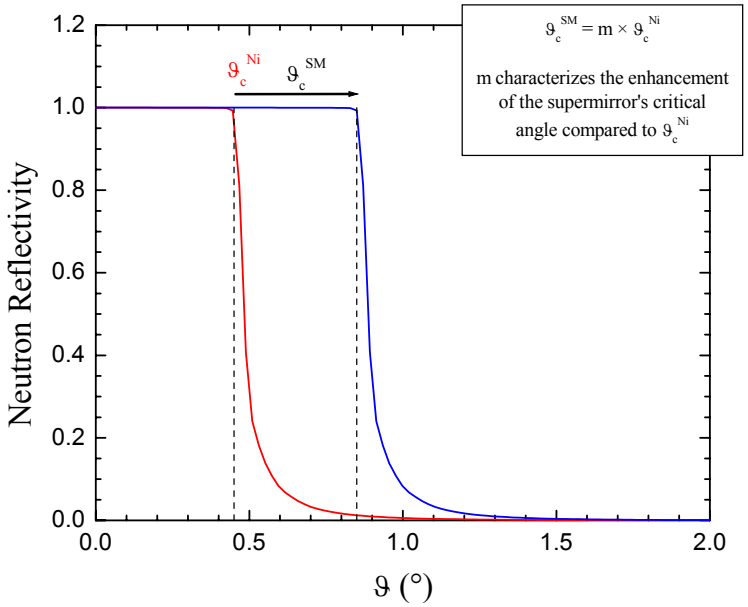

Fig. 11
Shift of the angle for total reflection by using a depth-graded multilayer system

4.2 TEM Image of a supermirror

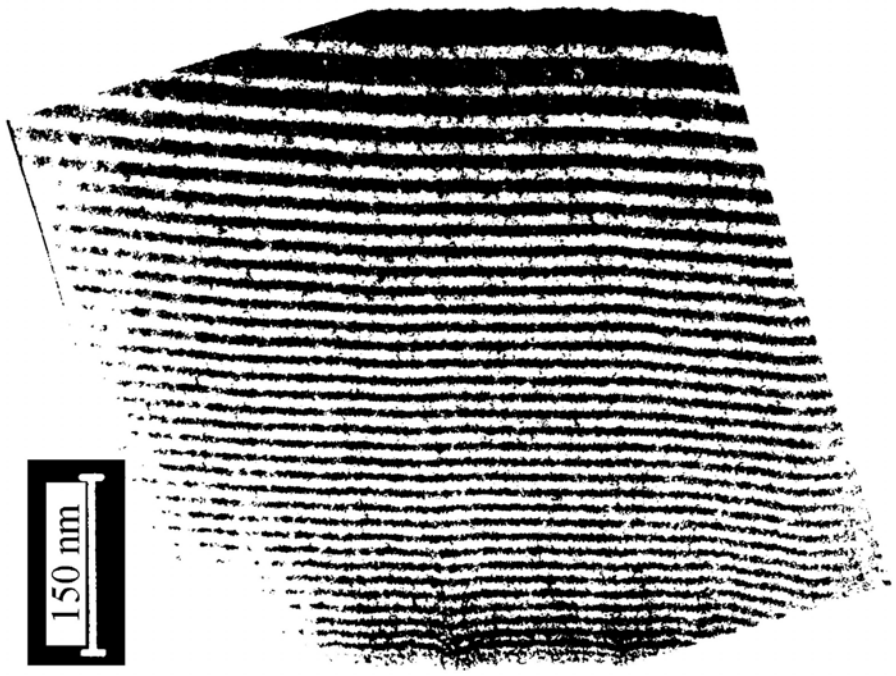

Fig. 12
TEM image of a supermirror

Fig. 12 shows an image of a real supermirror, taken with a transmission electron microscope.[8]

The depth-graded composition of the aperiodic multilayer, together with relatively sharp interfaces, is clearly visible. In some areas one can observe deviations from the desired perfectly flat stacking of the layers. These defects may result from local island growth of the thinnest layers or from dirt particles (or other defects) on the substrate surface.

In the following, two approaches for the design of supermirrors will be discussed.

4.3 Theoretical algorithms

Mezei gave the first design "recipe" for artificially increasing the total reflection region of a neutron mirror beyond the critical momentum transfer of Ni. His approach is based on the idea of a continuously depth-graded multilayer, which he named "supermirror".[9,10] The working principle is based on Bragg reflections of neutrons by a system of double layers with varying periodicity which interfere coherently resulting in a large increase of the critical angle.

Depth-graded multilayers have only limited coherence. The coherence isn't immediately lost, however, if the changes in bilayer thickness are not too drastic. Fig. 13 demonstrates this effect schematically.

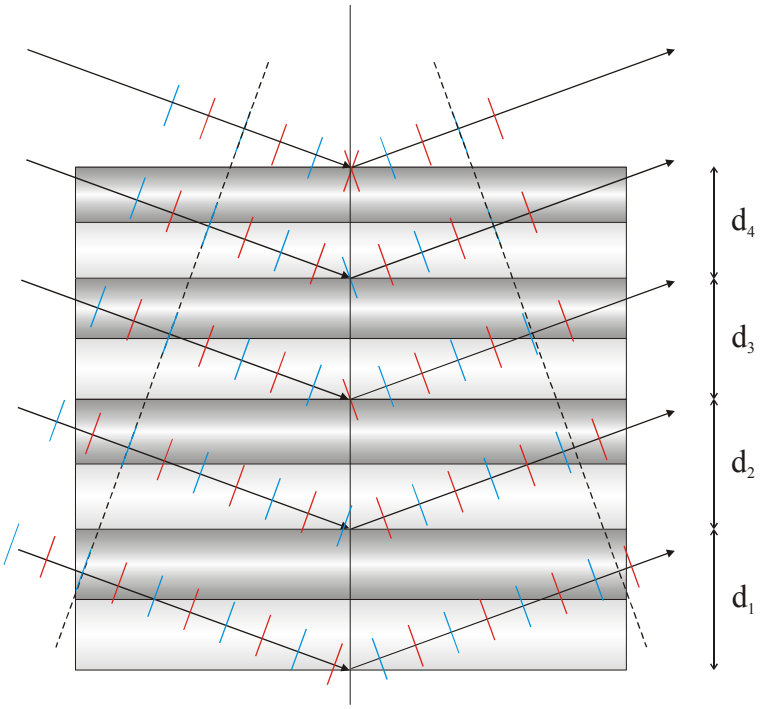

Fig. 13
Limited coherence in depth-graded multilayers

The incoming neutron wave is reflected at the interfaces of the supermirror. Partial waves that have been reflected by the upper and lower interface of bilayer 4 are exactly in phase. Since the bilayer thickness increases gradually ($d_4 < d_3 < d_2 < d_1$), the reflections at the d_3/d_2 boundary (and d_2/d_1 boundary etc.) get increasingly out of phase with the d_4/d_3 reflection. The different reflected waves are understand to be coherent as long as the phase shift is less than $\lambda/4$.

Depth-graded multilayers are most effective if materials are used which have as large as possible scattering contrast, i.e. Ni and Ti. The bilayer period has to be changed slowly enough such that at any momentum transfer below the critical q of the supermirror, a sufficiently large number of bilayers scatter the neutron waves "in phase", i.e. to within ± 45º phase difference, to result in almost total reflectivity. Since the multilayer is usually covered by a Ni capping layer (typically several 100 Å thick), the supermirror reflective effect needs only exist for $q > q_c^{Ni}$. In the limit of very large q_c values, corresponding to small bilayer periodicity, the individual single layer thicknesses must be equal for optimal supermirror performance. In this "continuum" regime, refraction effects can be neglected. However, in the large bilayer thickness limit, i.e. close to the critical q of Ni, refraction effects play a significant role, demanding a correction of individual layer thicknesses.[11,12] Mezei's derivation of the supermirror layer sequence is based only on the real part of the materials optical index. Extinction effects, however, influence the maximum achievable reflectivities, particularly for high-m supermirrors.

A more sophisticated algorithm developed by Hayter and Mook takes into account the discrete nature of the layers.[12] It is based on a determination of the contribution of a given bilayer to the overall reflectivity in a sequence of layers. This method can easily take extinction into account. To construct a supermirror stack, the thicknesses of successive bilayers are chosen such that their reflectivity profiles intersect at half height. The starting point is defined by the intersection of the profile of the thickest bilayer and the critical edge of the substrate or an additional capping layer. This approach allows predetermination of a "design reflectivity" function for the supermirror. Usually this function is chosen such that the reflectivity declines linearly from practically unity at q_c of Ni to the desired reflectivity at q_c of the supermirror. For a given number of bilayers in the supermirror structure, varying the design reflectivity function allows for either optimizing reflectivity over a correspondingly smaller q-range or increasing the m-value of the supermirror at the expense of reflectivity.

Fig. 14 illustrates the design of a supermirror. It shows how the neutron reflectivity of a Ni/Ti supermirror changes after sequentially increasing the numbers of bilayers. Film deposition usually starts with the thinnest layers on the well-polished glass or Si substrate (see upper part of Fig. 14) since the reflecting properties of those layers are most affected by roughness. In this example, an m=2 supermirror is calculated using Hayter and Mook's formula. In this case, 41 bilayers are required to achieve total reflection up to two times the critical edge of natural Ni (see lower part of Fig. 14). The first bilayer consists of 86.2 Å Ni / 72.1 Å Ti , whereas the 41st bilayer consists of 351.7 Å Ni / 123.2 Å Ti. Note that an extra 700 Å thick Ni capping layer is required to eliminate the reflectivity gap between of the critical edge of the substrate and the onset of the supermirror reflectivity at $q_c = 0.022 Å^{-1}$. The individual reflectivity curves have been calculated using a simulation program based on the well-known Parratt-formalism.[7] For simplicity, the effect of interface roughness has not been included in these calculations. This issue will be discussed separately in paragraph 5.5.

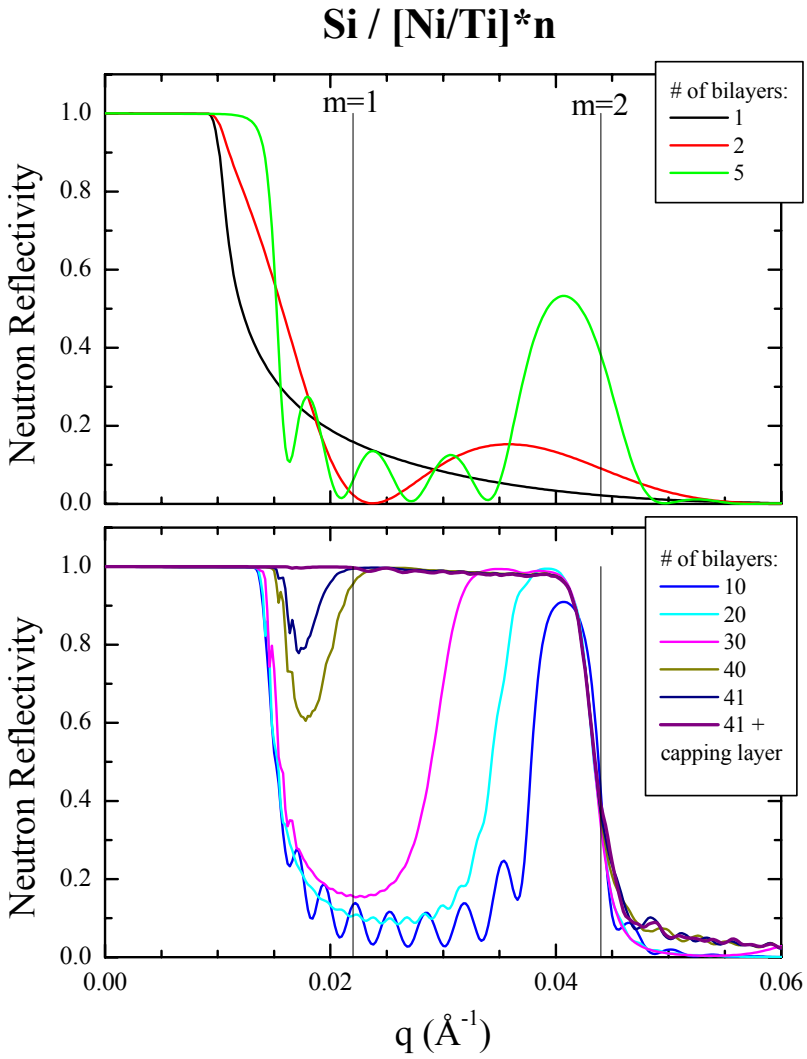

Fig. 14
Calculated reflectivity functions of an m=2 Ni/Ti supermirror after deposition of various numbers of bilayers

Fig. 15 shows calculated neutron reflectivity curves of m=2 Ni/Ti supermirrors following

1. Mezei's approach based on equally thick individual layers (black curve)
2. Mezei's approach corrected for refraction effects (red curve)
3. Hayter & Mook approach (green curve)

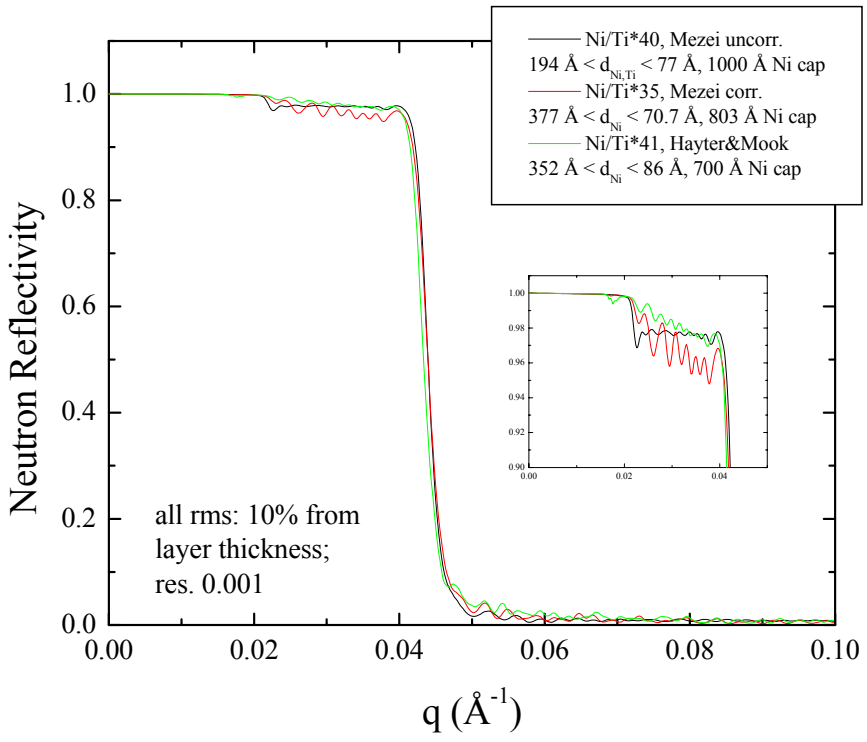

Fig. 15
Comparison of Mezei's and Hayter & Mook's supermirror design recipes

As can be seen, there are only marginal differences in reflectivity.

Tab. 1 lists the (rounded) individual layer thicknesses for an m=2 Ni/Ti supermirror for

1. Mezei's approach based on equally thick individual layers: **Mezei -uncorrected-**
2. Mezei's approach corrected for refraction effects: **Mezei - corrected-**
3. **Hayter & Mook**

m=2 Supermirror	Material	Mezei -uncorrected-	Mezei -corrected-	Hayter & Mook
Capping layer	Ni	1000	803	700
bilayer 1	Ti	194	135	123
	Ni	194	377	352
bilayer 2	Ti	163	124	119
	Ni	163	254	280
bilayer 3	Ti	147	117	115
	Ni	147	209	239
bilayer 4	Ti	137	111	112
	Ni	137	183	212
bilayer 5	Ti	130	107	109
	Ni	130	167	193
bilayer 6	Ti	124	103	106
	Ni	124	155	179
bilayer 7	Ti	119	100	103
	Ni	119	145	168
bilayer 8	Ti	115	98	101
	Ni	115	138	159
bilayer 9	Ti	112	95	99
	Ni	112	132	151
bilayer 10	Ti	109	93	97
	Ni	109	127	145
bilayer 11	Ti	107	91	96
	Ni	107	123	139
bilayer 12	Ti	104	90	94
	Ni	104	119	135
bilayer 13	Ti	102	88	93
	Ni	102	115	131
bilayer 14	Ti	100	87	91
	Ni	100	112	127
bilayer 15	Ti	99	85	90
	Ni	99	110	124
bilayer 16	Ti	97	84	89
	Ni	97	107	121
bilayer 17	Ti	96	83	88
	Ni	96	105	118
bilayer 18	Ti	94	82	87
	Ni	94	103	115

m=2 Supermirror	Material	Mezei -uncorrected-	Mezei -corrected-	Hayter & Mook
bilayer 19	Ti	93	81	86
	Ni	93	101	113
bilayer 20	Ti	92	80	85
	Ni	92	100	111
bilayer 21	Ti	91	79	84
	Ni	91	98	109
bilayer 22	Ti	90	79	83
	Ni	90	96	107
bilayer 23	Ti	89	78	82
	Ni	89	95	105
bilayer 24	Ti	88	77	81
	Ni	88	94	104
bilayer 25	Ti	87	76	81
	Ni	87	92	102
bilayer 26	Ti	86	76	80
	Ni	86	91	101
bilayer 27	Ti	85	75	79
	Ni	85	90	100
bilayer 28	Ti	84	74	79
	Ni	84	89	98
bilayer 29	Ti	84	74	78
	Ni	84	88	97
bilayer 30	Ti	83	73	78
	Ni	83	87	96
bilayer 31	Ti	82	73	77
	Ni	82	86	95
bilayer 32	Ti	82	72	76
	Ni	82	85	94
bilayer 33	Ti	81	72	76
	Ni	81	85	93
bilayer 34	Ti	80	71	75
	Ni	80	84	92
bilayer 35	Ti	80	71	75
	Ni	80	Si	91
bilayer 36	Ti	79		74
	Ni	79		90

m=2 Supermirror	Material	Mezei -uncorrected-	Mezei -corrected-	Hayter & Mook
bilayer 37	Ti	79		74
	Ni	79		89
bilayer 38	Ti	78		73
	Ni	78		88
bilayer 39	Ti	78		73
	Ni	78		88
bilayer 40	Ti	77		73
	Ni	77		87
bilayer 41	Ti	Si		72
	Ni			86
				Si

Tab. 1
Individual layer thicknesses (rounded) for an m=2 Ni/Ti supermirror

Design Approach	ΣNi	ΣNi + capping layer	ΣTi	Number of bilayers	Total supermirror thickness
Mezei -uncorrected-	3997.00 Å	4997.00 Å	3997.00 Å	40	8994.00 Å
Mezei -corrected-	4244.30 Å	5047.50 Å	3056.00 Å	35	8103.50 Å
Hayter & Mook	5321.97 Å	6021.97 Å	3606.65 Å	41	9628.62 Å

Tab. 2
Overview of m=2 Ni/Ti supermirror characteristics

5. Supermirror performance

In this chapter we will discuss parameters affecting the performance of supermirrors on the basis of Ni/Ti multilayers, in particular the number of bilayers, possibilities for isotope substitutions, interfacial roughness and other imperfections.

5.1 Number of bilayers

Fig. 16 illustrates that, for a given design reflectivity function, the number of bilayers basically defines the q_c-value of the supermirror. It shows calculated neutron reflectivity curves of bulk Ni, and Ni/Ti supermirrors with increasing number of bilayers (see label). The layer sequences were calculated using the Hayter & Mook approach. It can be seen in Fig. 17 (derived from results shown in Fig. 16) that the increase in q_c is non-linearly related to the number of bilayers. High-m values require increasingly larger numbers of bilayers. To achieve m=3, for example, 250 bilayers are needed.

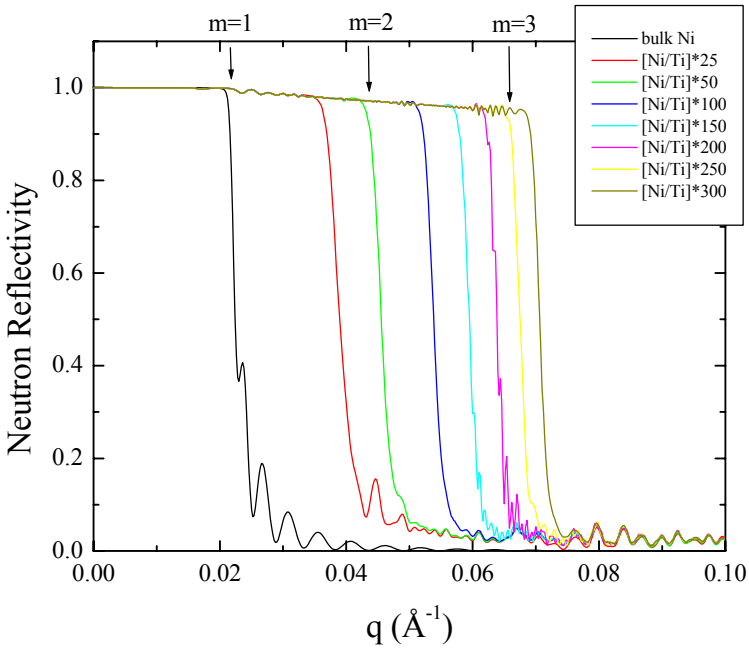

Fig. 16
Calculated neutron reflectivity of Ni/Ti supermirrors as function of number of bilayers

In our example the correlation between number of bilayers and q_c of the resulting supermirrors is approximately given by

$$\text{Number of bilayers} \sim 3 \times m^4 \qquad (4)$$

This function is plotted in Fig. 17. It is worthwhile to note that the exact relation always depends on the design reflectivity of the SM.

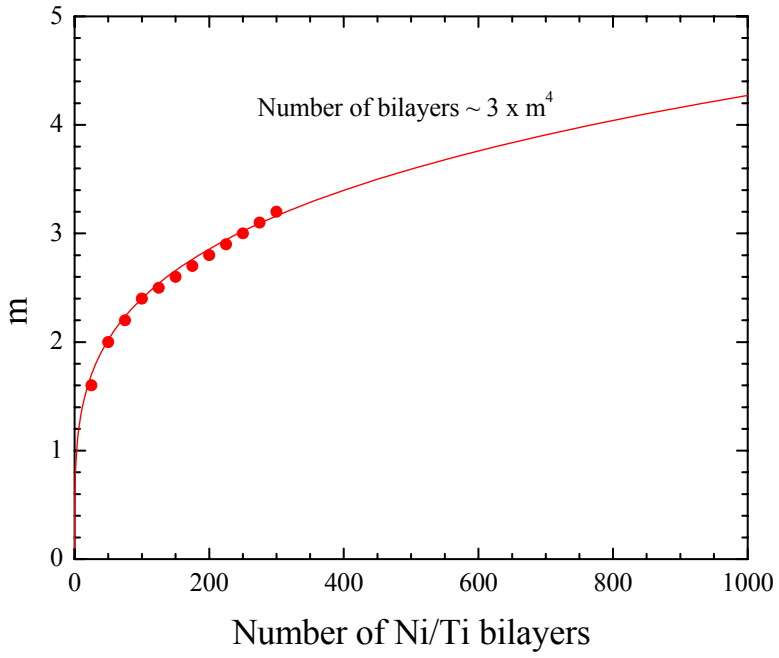

Fig. 17
Correlation between number of Ni/Ti bilayers and m-values of supermirrors

Fig. 17 also points out the requirement for adding more and more bilayers in order to reach very high critical q values. This approach is technically limited due to the following reasons:

i) With an increasing number of layers, quality correspondingly suffers due to the increasing amplification of interface roughness.
ii) Diffusion plays an increasing role especially for high-m supermirrors. The smallest single layer thickness of an m=4 supermirror is about 40 Å. For metallic multilayers, it is almost impossible to achieve rms-roughness values less than 5 Å.
iii) The technical demands and fabrication time needed for depositing high-m supermirrors is roughly proportional to the number of layers; therefore, the cost for high-performance supermirror coatings rises very steeply.
iv) The control of mechanical strain becomes more and more difficult for high-m supermirrors having very high total film thickness, e.g. approximately 35,000 Å in the case of m=3.5 mirrors. Associated with this is the danger of mechanical failure of the films (cracks or extensive peeling).

Therefore, it seems that m=4 should be considered as a practical limit for the m-value of supermirrors, at least with the deposition technology available today. In fact, m=4 supermirrors with 80% reflectivity at q_c have as yet only been produced on laboratory scale.[13] To the best of our knowledge, large area samples of these mirrors for actual applications have not reached more than 60% reflectivity.

5.2 Increasing/decreasing bilayer thickness

This chapter discusses the influence of the order of depth-graded bilayers.

In Fig. 18, the neutron reflectivity of an aperiodic multilayer with increasing bilayer thickness (from substrate to top) is represented by the black curve, for decreasing bilayer thickness by the red curve.

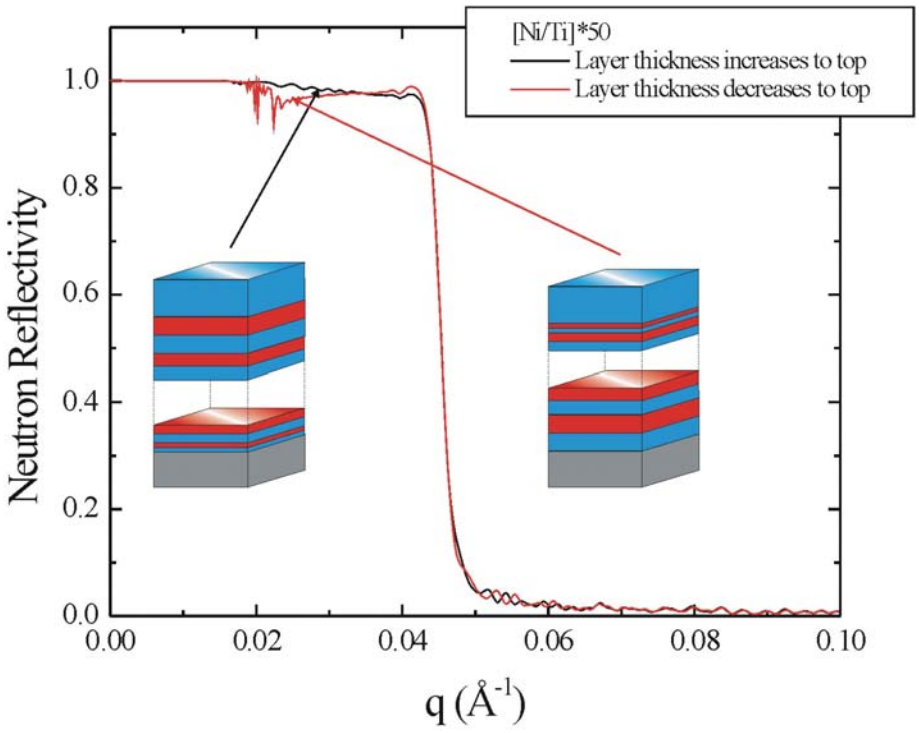

Fig. 18
Neutron reflectivity of an aperiodic multilayer with increasing and decreasing bilayer thickness from the substrate to the top, respectively

As can be seen, the black curve represents a marginal better performance in the q-range of 0.02 $Å^{-1} < q < 0.03$ $Å^{-1}$. This is due to absorption processes within the multilayers. In this q-range, the thick bilayers contribute most to the reflectivity. In case of decreasing bilayer thickness ratio, the neutron beam is already clearly reduced due to the absorption which takes place within the upper thinner layers (red curve).

But the thinner layers determine the reflectivity properties at the critical edge. Therefore, the red curve shows a slight increase of the reflectivity. If the thinner layers are on the top of the stack, absorption is less an issue at this q.

5.3 Reflectivity declension

Fig. 19 shows a theoretical reflectivity profile of a Ni/Ti supermirror with 50 bilayers (layer sequences were calculated using the Hayter & Mook approach).

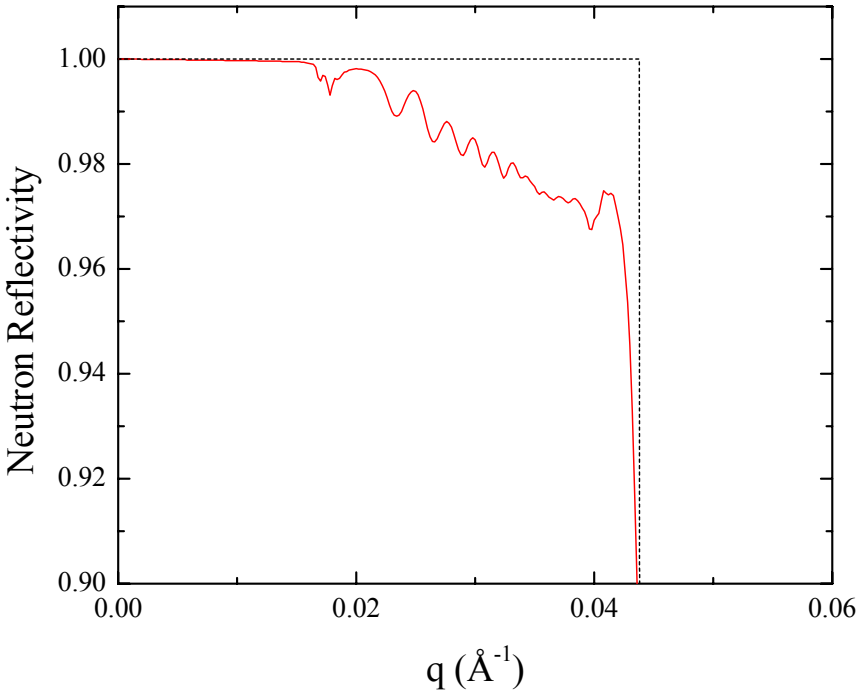

Fig. 19
*Neutron reflectivity of a [Ni/Ti]*50 multilayer*

For q < 0.017 Å^{-1}, the function is governed by the total reflectivity of the Ni capping layer (q_c^{Ni}). Above this value, the reflectivity is due to the supermirror coating. The latter has a q_c-value of 0.044 Å^{-1}.

At first glance, one might think that the supermirror reflectivity (approx. 98%) is sufficient because it's very close to unity. In reality, even a small deviation of the reflectivity from unity may have a strong impact on the instrument performance because depending on moderator emittance direction and wavelength, each neutron is bounced multiple times inside the guide system (typical numbers are 4-20 bounces). The decrease in intensity depends on the supermirror reflectivity and the number of bounces as

$$I(R, \#\text{ of bounces}) = I_0 \cdot R^{\#\text{ of bounces}}$$

as illustrated in Fig. 20.

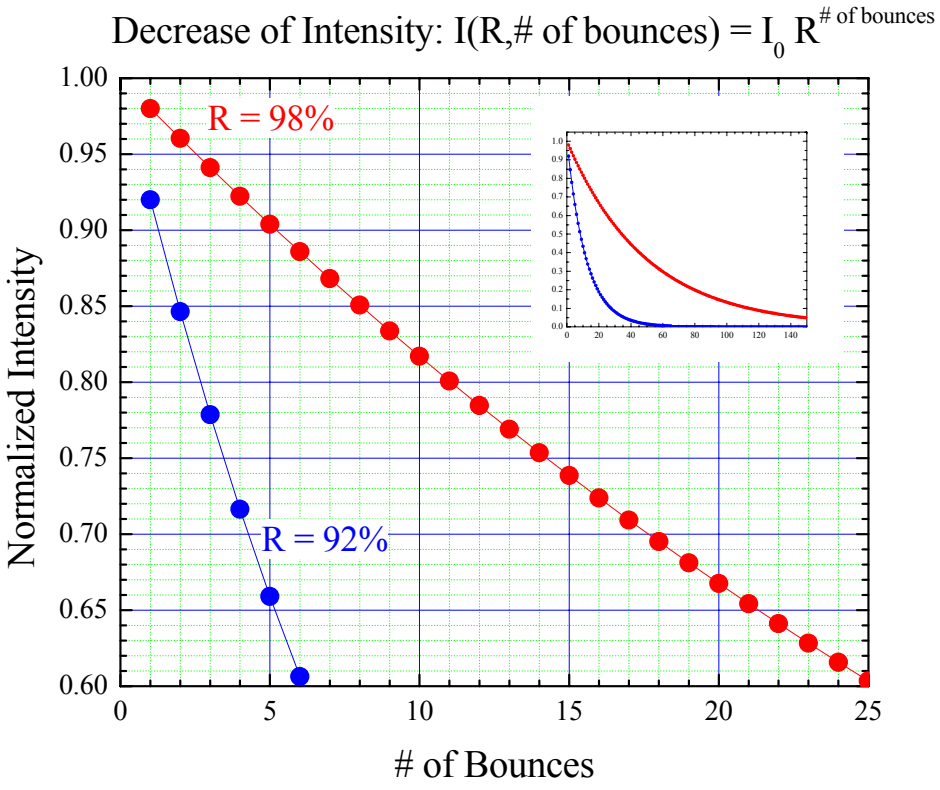

Fig. 20
Decrease of intensity during transportation of neutrons through a straight guide system

Assuming a reflectivity of 98%, after 5 bounces (which is a typical number for short instruments like the SNS reflectometers), the neutron intensity is already down to 90%. It's even worse when the supermirror shows a reflectivity of only 92%. After 5 bounces the neutron intensity is down to 66%.

The insert in Fig. 20 shows the behavior of this function for higher number of bounces. Thus, there's a good reason in trying to have the supermirror reflectivity as close to unity as possible.

5.4 Isotope substitution

Enhancement of the critical q-value of a supermirror and its reflectivity function may be achieved by artificially increasing the contrast in scattering length density, $\Delta N \cdot b$, between the materials A,B constituting the mirror. Tab. 3 lists $\Delta N \cdot b$ values for the cases in which natural Ni and Ti are substituted by more favorable isotopes or alloyed with other elements, for example hydrogen or carbon.

Material A	**N·b (10^{-6} Å^{-2})**		**Material B**	**ΔN·b (10^{-6} Å^{-2})**
Ni	9.4044	-1.945	Ti	11.3494
NiC	9.950	-1.945	Ti	11.8950
^{58}Ni	13.1479	-1.945	Ti	15.0929
^{58}Ni	13.1479	-3.4397	^{48}Ti	16.5876
^{58}Ni	13.1479	-6.0	TiH	19.1479
^{58}Ni	13.1479	-7.9435	^{62}Ni	21.0914

Tab. 3
Scattering length densities N·b of natural Ni and Ti, respectively, and possible isotope substitutions

Fig. 21 shows the effect of isotope substitution of the Ni layers for a Ni/Ti supermirror with 50 bilayers (in this case the Hayter & Mook formula has been used to calculate the layer sequence; absorption/incoherent scattering corrections have been included; each layer roughness was assumed to be 10% of that layer's thickness). As can be seen, there are significant improvements in m-value and reflectivity for the ^{58}Ni/Ti supermirror compared to the same mirror made of natural Ni and Ti.

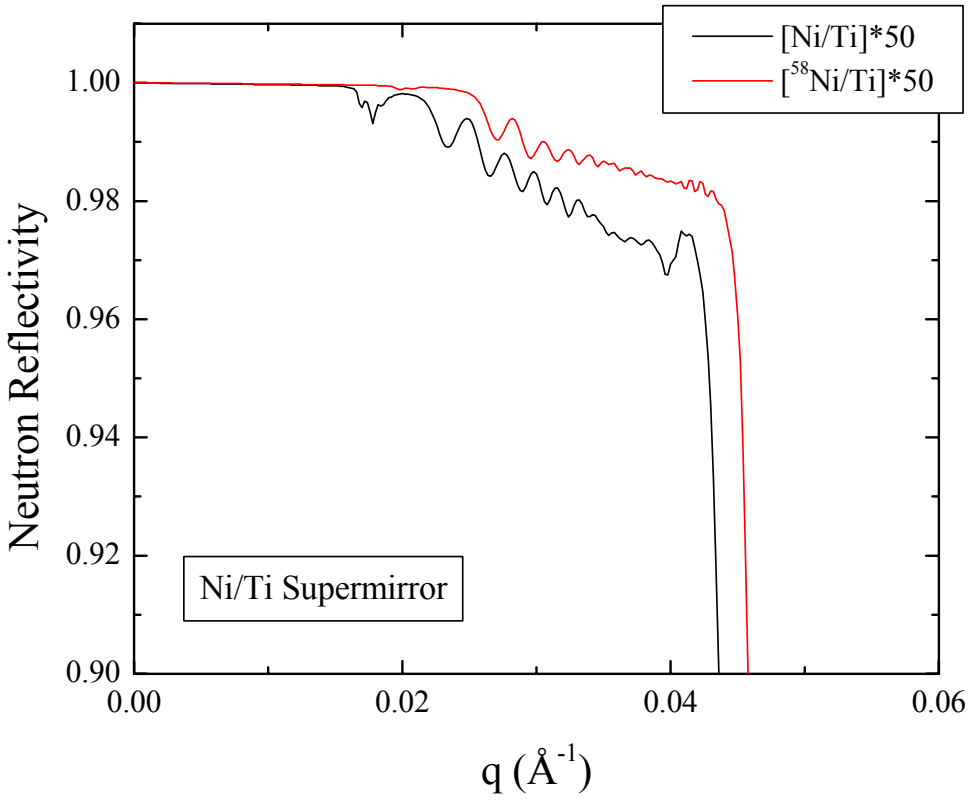

Fig. 21
Effect of isotope substitution in the Ni layers

Despite the attractive possibilities of improving a supermirror's performance by using isotopes, this approach has very high impact on production costs; therefore it is unlikely that isotope substitution will play a major role in large-scale production of supermirrors.

- Total thickness of Ni: 6770 Å = $0.677 \cdot 10^{-6}$ m

For 1 m^2 coating, $0.677 \cdot 10^{-6}$ m · m^2 Ni is needed.

$$\rho_{Ni} = 8.90 \frac{g}{cm^3} = 8.90 \cdot 10^6 \frac{g}{m^3}$$

$$\frac{8.90 \cdot 10^6 g}{m^3} = \frac{x}{0.677 \cdot 10^{-6} m^3}$$

$$\Rightarrow \underline{\underline{x = 6.0253 g}}$$

=> Total amount of Ni / m^2: **6.0253 g**

- Total thickness of Ti: 4240 Å = $0.424 \cdot 10^{-6}$ m

For 1 m^2 coating, $0.424 \cdot 10^{-6}$ m · m^2 Ti is needed.

$$\rho_{Ti} = 4.50 \frac{g}{cm^3} = 4.50 \cdot 10^6 \frac{g}{m^3}$$

$$\frac{4.50 \cdot 10^6 g}{m^3} = \frac{x}{0.424 \cdot 10^{-6} m^3}$$

$$\Rightarrow \underline{\underline{x = 1.908 g}}$$

=> Total amount of Ti / m^2: **1.908 g**

Tab. 4 shows an estimation of supermirror material costs, and costs for coating (based on vendor information).

Material	Quality	Material costs per m^2	Costs for coating per m^2 (materials + deposition)
Ni/Ti	m=2	~ $ 30	$ 10,000
	m=3	~ $ 100	$ 20,000
^{58}Ni / ^{48}Ti	m=2	~ $ 10,000	$ 20,000
	m=3	~ $ 25,000	$ 45,000

Tab. 4
Overview of supermirror costs (estimation based on vendor information)

The given numbers for materials cost do not include unavoidable losses that occur during the deposition process. Not all material that has been sputtered off the cathodes will actually be accumulated in the films. Some fraction will end up being scattered towards the walls of the chamber or other places.

5.5 Interface roughness and other imperfections

Supermirrors with 3.6 times the critical q of Ni became commercially available only recently after years of R&D at Paul Scherrer Institute (PSI) / Switzerland. A general drawback of high-m mirrors is that the reflectivity function of these coatings is far from being perfect (to a lesser extent this is also true for lower-m supermirrors, e.g. m=2 and m=3). In large-scale production of m=3.6 supermirrors, typical reflectivities of R=0.6-0.7 are reached at q_c. Theoretically, assuming a perfect layering, the reflectivity function should be considerably higher, on the order of 90% at q_c (absorption due to the enormous total thickness of approximately 35,000 Å and incoherent scattering are taken into account in the calculations). Obviously, large performance losses are caused by imperfections at the Ni/Ti interfaces and by the surface roughness of the substrate. So far, interface diffusion is thought to be the main reason for the low measured reflectivities; however, there might be other contributing factors that are not yet well investigated, for example small-angle scattering on the grain structure. Major distortions to the reflectivity may also result from limited coherence due to deviations from the design layer thicknesses, as was pointed out by Mezei.[11] It seems to be quite a challenge to keep the positions of the interfaces close to the nominal values in order to maintain coherent interference, particularly for supermirrors with very high m-values and the corresponding small individual layer thicknesses. For example, in the case of an m=3.5 supermirror, about 26 coherently reflecting bilayers are required for optimum reflectivity at q_c (where the individual layer thicknesses are about 40 Å). In order to satisfy the ± 45° phase difference criteria (cf. paragraph 4.3), offsets of actual positions of interfaces must be less than 10 Å.

There have been some suggestions recently to avoid amplification of interface roughness that occurs naturally when several hundred bilayers are being deposited. One idea is to smooth the layers after a certain fraction of the total deposition process. For example, Soyama et al. have applied ion polishing in combination with ion beam sputtering.[14] They achieved a decrease in the rms roughness of Ni films by ion-polishing from 6.5 Å to 3.5 Å.

5.6 Theory vs. Reality

In Tab. 5, calculated neutron reflectivities at the critical q value are compared with state-of-the-art supermirrors. The reflectivity values for m>1 are taken from literature.[15]

Supermirror Quality	$R_{theor.}$*	R_{real}
m=1	0.99	0.99
m=2	0.97	0.85
m=3	0.95	0.75
m=3.5	0.92	0.70
m=4	0.91	0.60

***Absorption, incoherent scattering, and interdiffusion/roughness (10% of layer thickness) taken into account!**

Tab. 5
Comparison of theoretically expected and "real" Ni/Ti supermirror reflectivity

An example for the large discrepancies between R_{real} and $R_{theor.}$ is illustrated in Fig. 22 which shows the measurement of an actual m=3.5 supermirror consisting of 600 Ni/Ti bilayers, being produced at PSI (red curve), together with the theoretical curve for this mirror (black curve).

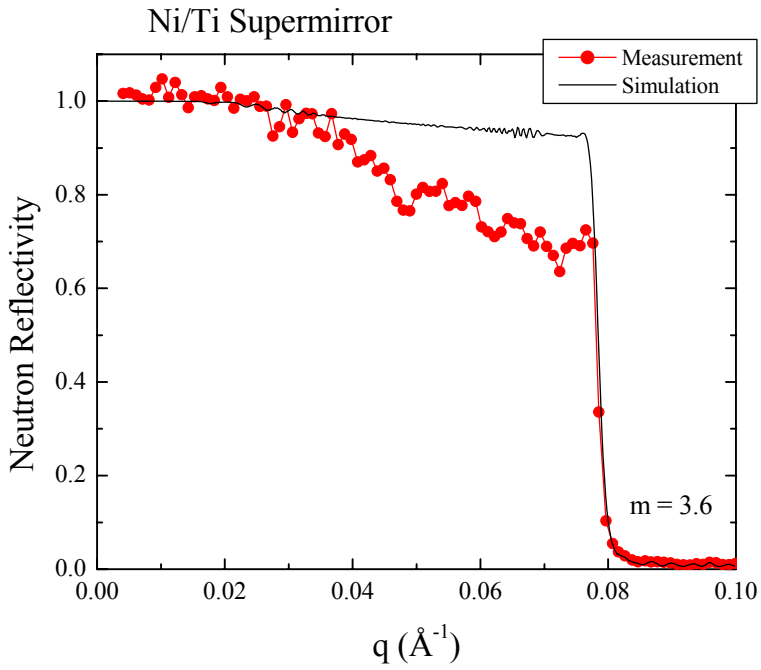

Fig. 22
Comparison of state-of-the-art supermirror quality and its theoretically expected performance

Loss mechanisms already taken into account in the calculations shown here are

- Absorption due to the enormous total thickness of approximately 50.000 Å
- Incoherent scattering (playing an important role)
- Roughness between the interlayers (10% of individual layer thickness), plus surface roughness of the substrate

As can be seen, additional loss mechanisms have to exist. Possibilities are:

- Interdiffusion among the layers becoming increasingly more important with decreasing layer thickness
- Limited coherence due to deviations from design layering
- Small-angle scattering on grain structure

By overcoming the losses stated above, **supermirror performances could be enhanced significantly**. An ongoing study addresses this subject, and investigates possibilities on how to reach theoretically expected neutron reflectivities.

6. Performance gains for the SNS Magnetism Reflectometer

This chapter demonstrates possible gains in instrument performance that may be achievable by improving high-m supermirror coatings. The proposed SNS Magnetism Reflectometer serves as an example. The basic layout of this instrument is illustrated in Fig. 23. Neutrons from the cold liquid hydrogen moderator are guided to the sample position at an 18 m distance via a combination of a channel beam bender and a tapered neutron guide. The bender (length: 5 m) is used to minimize high-energy neutron background at the sample position. It deflects the useful part of the wavelengths distribution ($\lambda > 1.5$ Å) by 2º horizontally and feeds it into a 9 m long focusing section, which compresses the beam size to match a typical sample size of 25 mm^2. High-energy neutrons cannot follow this curvature and are scattered and absorbed by appropriate shielding. Neutrons scattered by the sample will be counted by a two-dimensional multidetector at a 19 m distance from the moderator. The wavelength is determined by time-of-flight. The instrument is designed for 60 Hz operation, the normal source frequency of SNS. Bandwidth choppers restrict the total bandwidth of neutrons that are incident onto the sample to $\Delta\lambda = 3.5$ Å. If, for example, the most intense wavelength band from 2.6 Å to 6.1 Å is used for data collection at the SNS instrument, a neutron flux of approximately 3.7 x 10^9 neutrons/cm^2/s (at guide exit) can actually be used for concurrent data collection.

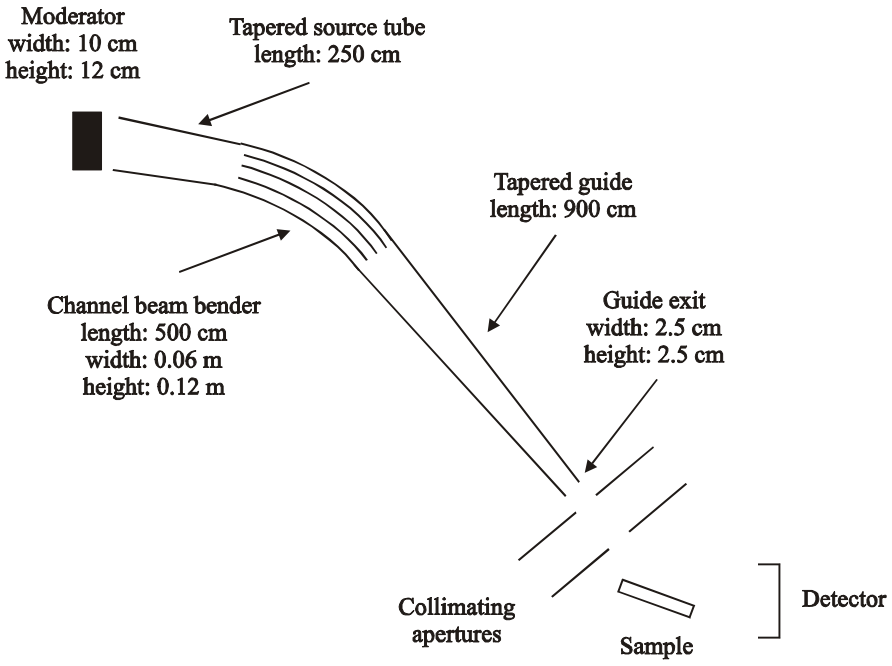

Fig. 23
Schematic layout of Magnetism Reflectometer to be built at SNS (top view)

The neutron guide system of the instrument has been optimized by Monte Carlo (MC) simulations using the program IDEAS.[16] The above stated flux number implies that m=3.5 supermirrors with 65% reflectivity at the critical edge will be utilized for all guide surfaces. This specification is challenging but does not seem to be beyond the capabilities of current guide vendors.

Fig. 24 shows the effect of varying the reflectivity value (at q_c) for the above instrument configuration in the wavelength range up to 14 Å. In order to reflect a realistic situation in which large guide gains can be expected, we calculate flux on sample for a low-resolution experiment. In this case a highly divergent beam can be utilized. In particular, we assume: 25 mm x 25 mm sample size, 20° incident angle, and 10% angular resolution. The latter is achieved by using a pair of slits with 0.5 m distance from each other, which is located between the exit of the tapered guide and the sample position. The intensities displayed in Fig. 24 have been integrated over 5% wide neutron wavelength bins. Note that the sharp wavelength cut off at about 2 Å results from using the beam bender.

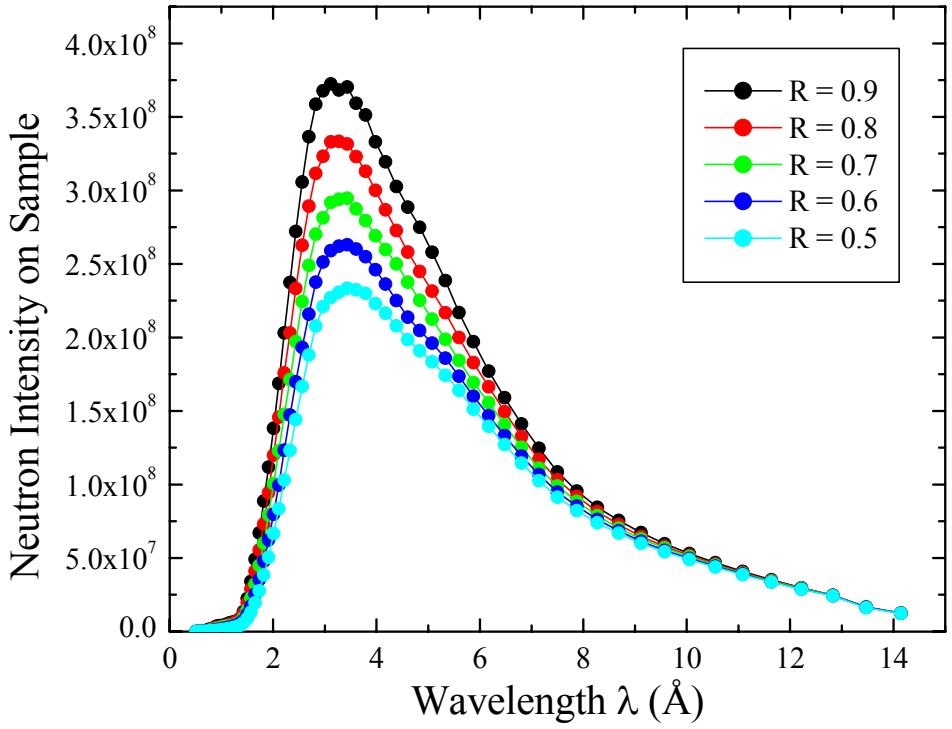

Fig. 24
Effect of different reflectivity (R) values (at q_c) for m = 3.5 supermirrors used as coating in the Magnetism Reflectometer neutron guide. The reflectivity function between q_c(Ni) and q_c(supermirror) was assumed to be linear

Fig. 25 shows the enhancement in flux-on-sample that may be achievable if supermirrors with higher reflectivity at q_c could be produced in large quantities. The intensity gain functions have been obtained by normalizing the flux values of Fig. 24 relative to the R=0.5 data. It can be seen from Fig. 25, that the short wavelength intensity in particular would be significantly increased.

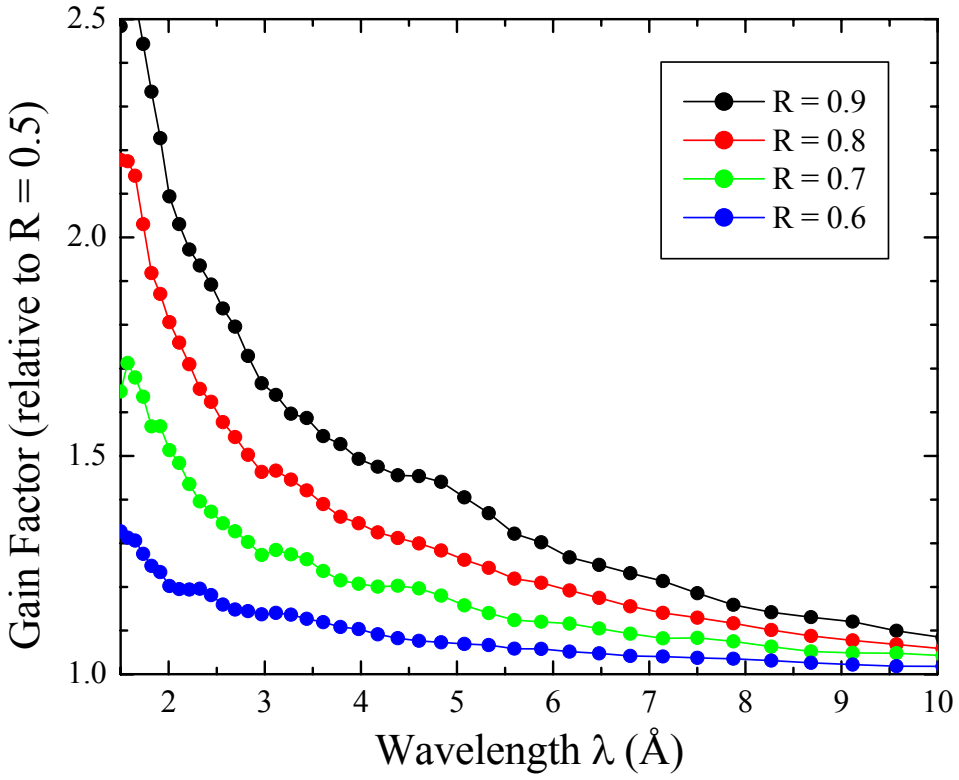

Fig. 25
Neutron intensity gain of various supermirror guide coatings (with different R-values at q_c) relative to an R=0.5 coating

7. Acknowledgments

The authors are thankful to T. Krist, D. Clemens, and P. Boeni for sharing their knowledge about supermirrors. Valuable discussions with C. Prokuski in preparing this manuscript are also gratefully acknowledged. This work is supported by the U.S. Department of Energy under contract No. DE-AC05-000R22725 (SNS Project).

8. References

[1]T.E. Mason, T.A. Gabriel, R.K. Crawford, K.W. Herwig, F. Klose, and J.F. Ankner, "The Spallation Neutron Source: A powerful tool for materials research", published on the Los Alamos National Laboratory e-print server, available at http://arXic.org/format/physics/0007068.

[2]R.K. Crawford, "Neutron scattering instrumentation - A guide to future directions", Proc. of ICANS-XV, pp. 61-68, 2000.

[3]J. Christ, and T. Springer, "The development of a neutron guide at the FRM reactor", Nukleonik 4, pp. 23-25, 1962.

[4]Brochure "The Spallation Neutron Source SINQ", Paul Scherrer Institute, Switzerland.

[5]P. Boeni, D. Clemens, M. Senthil Kumar, and S. Tixier, "Challenges in the field of large-m supermirrors", Physica B 241-243, pp. 1060-1067, 1998.

[6]L. Névot and P. Croce, Rev. Phys. Appl. 15 (1980) 761

[7]Parratt 32 - The Reflectivity Tool 1.5.2, Christian Braun, Hahn-Meitner Institute Berlin, Germany.

[8]D. Clemens, Thesis, Technical University Berlin, Germany, 1993.

[9]F. Mezei, "Novel polarized neutron devices: Supermirror and spin component amplifier", Comm. Phys. 1, pp. 81-85, 1976.

[10]F. Mezei and P.A. Dagleish, "Corrigendum and first experimental evidence on neutron supermirrors", Comm. Phys. 2, pp. 41-43, 1977.

[11]F. Mezei, "Multilayer neutron optical devices", Physics, Fabrication, and Applications of Multilayered Structures, pp. 311-333, Plenum Press, New York and London, 1987.

[12]J.B. Hayter and H.A. Mook, "Discrete thin-film multilayer design for X-ray and neutron supermirrors", J. Appl. Cryst. 22, pp. 35-41, 1989.

[13]ILL News for Reactor Users 31, p.12, June 1999.

[14]K. Soyama, W. Ishiyama, and K. Murakami, "Enhancement of reflectivity of multilayer neutron mirrors by ion polishing", JAERI-Review 2000-005, p. 57, 2000.

[15]See for example: P. Boeni, Physica B 234-236 (1997) 1038-1043; M. Senthil Kumar et al., Physica B 241-243 (1998) 95-97; P. Boeni, Physica B 241-243 (1998) 1060-1068

[16]IDEAS, Wai-Tung Lee, Oak Ridge National Laboratory.